



HAL
open science

Modelling study of emulsion latex coagulation processes in coagulators

Dang Cheng, Nida Sheibat-Othman, Timothy Mckenna

► **To cite this version:**

Dang Cheng, Nida Sheibat-Othman, Timothy Mckenna. Modelling study of emulsion latex coagulation processes in coagulators. *Canadian Journal of Chemical Engineering*, 2020, 10.1002/cjce.23851 . hal-02992613

HAL Id: hal-02992613

<https://hal.science/hal-02992613>

Submitted on 25 Nov 2020

HAL is a multi-disciplinary open access archive for the deposit and dissemination of scientific research documents, whether they are published or not. The documents may come from teaching and research institutions in France or abroad, or from public or private research centers.

L'archive ouverte pluridisciplinaire **HAL**, est destinée au dépôt et à la diffusion de documents scientifiques de niveau recherche, publiés ou non, émanant des établissements d'enseignement et de recherche français ou étrangers, des laboratoires publics ou privés.

Modelling study of emulsion latex coagulation processes in coagulators

Dang Cheng¹, Nida Sheibat-Othman², Timothy F.L. McKenna¹

1. *Université Claude Bernard Lyon 1, CPE Lyon, CNRS, UMR 5265, Laboratoire de Chimie, Catalyse, Polymères et Procédés (C2P2)-LCPP group, Villeurbanne, France*

2. *University of Lyon, Université Claude Bernard Lyon 1, CNRS, LAGEPP UMR 5007, Villeurbanne, France*

Abstract: This paper presents a numerical study of emulsion latex coagulation processes in continuous coagulators based on the full computational fluid dynamics approach. The RANS approach together with the k - ε turbulence model was used to describe the detailed flow field in the coagulators. The coagulant mixing process was modelled by the convection-diffusion equation and the emulsion latex coagulation process was formulated by the population balance equation of the particle size with a coagulation kernel including a perikinetic and orthokinetic combined mechanism. The flow and coagulation models were independently validated by means of comparing simulated results to the relevant experimental data from the literature. A series of simulations were carried out to study the effects of coagulator bottom shape, salt solution feeding location, residence time and agitation speed, as well as the influence of four typical scale-up criteria on the latex particle coagulation process. The presented results would be helpful for the relevant process design, development and scale-up of continuous latex coagulators.

Keywords: computational fluid dynamics; mixing; emulsion latex coagulation; particle size distribution

1. Introduction

Emulsion polymerization is a technology widely used to produce synthetic materials such as adhesives, paints, rubber, textile products, binders and protective coatings in the form of a colloidal dispersion of nanoparticles (i.e., latex). In applications where the latex is to be used under the form of dispersions, one of the crucial characteristics that would affect the end-use properties of latex products is the particle size and particle size distribution (PSD), such as the rheological behavior, drying characteristics, optical properties, film-forming properties and mechanical strength, etc. ^[1]. In applications where the latex particles are to be recovered separately from the continuous phase under the form of a powder that can be more easily processed, it is preferable to coagulate the nanoscale particles as fine particles less than 10 microns in diameter pose health and safety problems, can be lost in the downstream recovery process, or may cause problems when processing the recovered resin powder into pellets ^[2]. In addition, the PSD also affects the reaction rate considerably, therefore, ensuring the particles stability during the polymerization process is essential (usually submicronic particles are aimed). When one needs particles larger than those produced directly in the polymerization process, a coagulator can be installed after the polymerization reactor into which the resultant latex is pumped, and a well-controlled particle coagulation is triggered in the coagulator in order to modulate the PSD.

The latex particles are usually stabilized via the addition of one or more surfactants. The choice of surfactant is out of the scope of this text, but generally they fall into one of two categories: ionic and non-ionic surfactants. In many commercial applications one would find a single anionic surfactant for reasons of process simplicity and cost. In this case the surface of the particles carries (negative) electrical charges that repulse the same charges on neighboring particles. The idea is that this repulsive potential energy

should be higher than the attractive forces or inertia energy that the particles might have, thereby preventing particles from entering into contact with each other and coagulating.

As the latex particles are on the scale of nanometers, two major mechanisms may drive the particle coagulation process: one is the Brownian motion of particles (i.e., perikinetic mechanism), which constantly brings them into close proximity with other; the other is the motion of fluid (i.e., orthokinetic mechanism), which enhances the collision frequency of the latex particles. Both mechanisms co-exist in a coagulator, but the extent to which one of them is dominant depends on the operating conditions in the coagulator. In other words, the effect of mixing on the coagulation rate may be negligible for a low agitation rate for well-stabilized particles, or dominant at high shear rates. Therefore, both the Brownian and the fluid motions cause particle collision, but the coagulation efficiency is determined by the stabilization of the particles that counterbalances these forces.

In principle, the particle coagulation process can be accelerated in two ways: increasing the collision frequency of latex particles by agitation, or by reducing the magnitude of the inter-particle repulsive potential energy (i.e. increasing the coagulation efficiency) by injecting a coagulation agent (i.e., coagulant) such as a salt solution or an acid (e.g., sulfuric acid or sodium chloride). Indeed, the coagulation process in a coagulator is influenced by the combined effect of perikinetic and orthokinetic mechanisms and thus can be controlled by manipulating both of them.

In the current work, we focused on the continuous latex coagulator, which constitutes an important unit operation in emulsion polymerization industry, as schematically shown in Figure 1 [2]. The latex leaving the polymerization reactor is continuously fed into the agitated coagulator, and a separate stream is used to inject the coagulant. As the

involved chemical processes and inter-particle interaction are intimately coupled with the complex transport phenomena in the coagulator, its efficient design, optimization and scale-up still represents a big challenge.

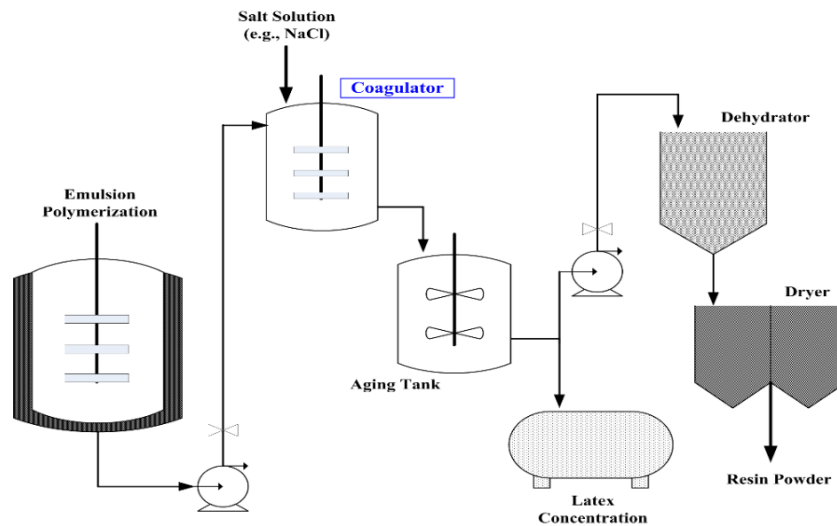


Figure 1. Flow diagram for the typical emulsion polymerization.

Mathematical modelling can play an important role in comprehending the effect of various operating conditions on the final PSD, and hence facilitates the process design and improvement in this regard ^[3, 4]. In general, modelling works in the area of emulsion polymerization has paid more attention to the nucleation and growth during latex production, while only a limited number of works have dealt with coagulation phenomenon, especially in coagulators. Among the efforts made to model the emulsion polymer coagulation process in the literature in order to predict the PSD, the vast majority have adopted the dynamic modelling approach incorporating the perikinetic coagulation mechanism ^[2, 5-23]. Some other studies attempted to deal with the orthokinetic coagulation in a semi-empirical manner ^[24-27]. All these works were based on the assumption of perfect mixing within coagulators, in which spatially averaged

coagulant concentrations and shear rates were adopted. However, in reality, the coagulant concentration and shear rate vary spatially in a coagulator, especially in a pilot or large-scale coagulator. The energy dissipation rate and shear rate near the impellers are known to be thousands of times higher than those in regions away from the impellers, even in a bench scale batch coagulator (see for instance reference ^[28]). Such inhomogeneities can play a significant role in determining mass and heat transfer conditions, shear-induced particle coagulation, and may lead to different local values of the dynamic viscosity of the dispersions if they have a strongly non-Newtonian character ^[29-31]. This latter point is especially prominent for high solid content (HSC) latexes.

Computational fluid dynamics (CFD) is capable of analyzing detailed flow fields and local mixing characteristics. Modelling of latex coagulation based on the CFD approach is hence expected to provide a deeper insight into the process. Several attempts were reported in the literature to model particle coagulation using the CFD approach to account for the local turbulence and coagulant concentration in batch coagulators ^[3] and semi-batch emulsion polymerization reactors ^[4, 32, 33]. Pohn et al. ^[4, 32] developed a computational framework combining CFD with a multi-zonal population balance model to simulate the semi-batch emulsion polymerization and applied ^[33] the framework to investigate the scale-up production of polymer latexes with bimodal particle size distributions. Nevertheless, only perikinetic coagulation was taken into account and the population balance model was only resolved in nine zones in their work ^[4, 33]. Elgebrandt et al. ^[3] calculated the shear-induced coagulation in batch coagulators by implementing the local turbulent energy dissipation rates obtained from CFD approach and indicated that the results were different as compared to those based on the spatially-averaged turbulent energy dissipation rates.

Modelling of coagulation processes in continuous latex coagulators has rarely been dealt with, especially based on the full CFD approach. Considering the fact that the process design and optimization for continuous latex coagulators are still limited by a lack of knowledge of the influences of relevant operating conditions and scale-up on the relevant particle coagulation processes. Therefore, the aim of this paper is to first develop an in-house numerical simulation tool to describe the latex coagulation process in continuous coagulators. Then, numerical simulations were carried out to study the effects of coagulator bottom shape, salt solution feeding location, residence time, agitation speed, and four typical scale-up criteria on the latex particle coagulation processes. The series of simulations carried out are expected to provide a guideline for process design, development and improvement of this industrially important unit reactor.

2. Coagulation modelling

2.1 Population balance equation

The evolution of latex PSD caused by particle coagulation in a coagulator is modelled by a population balance equation (PBE) as

$$\frac{\partial n(V,t)}{\partial t} + \nabla \cdot [\mathbf{u}n(V,t)] - \nabla \cdot [\Gamma_{eff} \nabla n(V,t)] = -n(V,t) \int_{V_0}^{\infty} \beta(V,V') n(V',t) dV' + \frac{1}{2} \int_{V_0}^{V-V_0} \beta(V-V',V') n(V-V',t) n(V',t) dV' \quad (1)$$

where the PSD is expressed as number density function $n(V,t)$, $\beta(V,V')$ is the coagulation rate coefficient between particles of volumes V and V' , V_0 is the smallest volume of particles, \mathbf{u} is the velocity vector and Γ_{eff} is effective diffusivity.

The evaluation of $\beta(V,V')$ is a prerequisite for solving Eq. (1).

Both the perikinetic and orthokinetic mechanisms coexist in a coagulator. Smoluchowski^[34] developed a perikinetic model, to which the stability ratio (W_{ij}) was added later as^[35]

$$\beta(r_i, r_j) = \frac{2k_B T}{3\mu W_{ij}} (r_i + r_j) \left(\frac{1}{r_i} + \frac{1}{r_j} \right) \quad (2)$$

where r_i and r_j are the radii corresponding to particle volumes of V and V' , and the colloidal stability ratio W_{ij} is the inverse of the collision efficiency^[35]

$$W_{ij} = (r_i + r_j) \int_{r_i+r_j}^{\infty} \frac{e^{\frac{V_{\text{int}}}{k_B T}}}{R^2} dR \quad (3)$$

where R is center-to-center separation distance and V_{int} is the total inter-particle interaction. The stability ratio was modified as follows in order to account for the shear forces^[36, 37]

$$W_{ij, \text{com}} = (r_i + r_j) \int_{r_i+r_j}^{\infty} \frac{e^{\left(\frac{V_{\text{int}}}{k_B T} - \frac{4Pe(r_i+r_j)}{3\pi R} \right)}}{R^2} dR \quad (4)$$

where Pe is particle Peclet number traditionally defined as^[38, 39]

$$Pe = \frac{3\pi\mu\dot{\gamma}(r_i + r_j)}{2k_B T} \quad (5)$$

where $\dot{\gamma}$ is the shear rate. It can be seen that the Peclet number determines the relative magnitude of orthokinetic coagulation to perikinetic coagulation. A modified Peclet number (Pe') was later proposed to account for the effect of ionic strength as^[40]

$$Pe' = Pe \frac{1 + \kappa r}{(\kappa r)^2} \quad (6)$$

where κ is the Debye-Huckel parameter and $r = \frac{r_i + r_j}{2}$.

2.2 Inter-particle interactions

The colloidal properties of emulsion latexes are determined by the inter-particle interactions between particles. Since the latex is considered to be stabilized by an anionic surfactant in the current work, the so-called electrical double layer (EDL) is formed around the surface of each individual latex particle, which is composed of the inner Stern layer and the outer diffuse layer^[41]. On the basis of this representation, the Derjaguin-Landau-Verwey-Overbeek (DLVO) theory^[41] was used to account for the inter-particle interactions including the van der Waals attraction (V_A) and repulsion (V_R) due to electrostatic charges on the particle surface in latexes stabilized by ionic surfactant. The total inter-particle interaction (V_{int}) is the sum of the van der Waals attraction and the electrostatic repulsion between two particles

$$V_{\text{int}} = V_A + V_R \quad (7)$$

The van der Waals attraction is given by

$$V_A = -\frac{A}{6} \left[\frac{2r_i r_j}{R^2 - (r_i + r_j)^2} + \frac{2r_i r_j}{R^2 - (r_i - r_j)^2} + \ln \left(\frac{R^2 - (r_i + r_j)^2}{R^2 - (r_i - r_j)^2} \right) \right] \quad (8)$$

where A is the Hamaker constant, and the value reported by Evans and Napper^[42] was employed in this work.

In the representation of electrical double layer, the anionic surfactant adsorbs onto the particle surface, while a portion of counterions adsorb between the particle surface and the inner Helmholtz plane (IHP). However, it is charge free in the sub-layer between IHP and the outer Helmholtz plane (OHP). Therefore, the net charge at OHP can be calculated as^[11]

$$\sigma_d = \sigma_0 - \sigma_i \quad (9)$$

where σ_0 is charge density at particle surface due to the adsorption of anionic surfactant, σ_i is the total charge of counterions adsorbed at IHP. Correspondingly, the potential at IHP is ϕ_i and at OHP is ϕ_d , and the two potentials are correlated as ^[11]

$$\phi_i - \phi_d = \frac{\sigma_d}{K_s} \quad (10)$$

where $K_s = \frac{\varepsilon_s}{4\pi\delta}$ is the capacitance of the sub-layer, ε_s the permittivity of the Stern layer and δ is the thickness of outer Stern layer.

The repulsive force arises when two charged particles approach each other, which is directly determined by the potential of ϕ_d at OHP. The potential ϕ_d is equivalent to the electrokinetic potential (ζ) in this context. The electrokinetic potential (ζ) for $kr < 1$ can be approximately related to σ_d and κ as ^[11]

$$\phi_d = \frac{4\pi r \sigma_d}{\varepsilon(1 + \kappa r)} = \zeta \quad (11)$$

For $kr \geq 1$, the electrokinetic potential (ζ) is related to σ_d and κ as

$$\phi_d = \frac{2k_B T}{e} \sinh^{-1} \left(\frac{2\pi r e \sigma_d}{\varepsilon \kappa k_B T} \right) = \zeta \quad (12)$$

The coagulators are often operated under conditions of low potential and thin double layer (i.e., $\frac{1}{\kappa r} \ll 1$), in such cases the electrostatic repulsion can be approximated by

the HHF (Hogg, Healy & Fuerstenau) expression as ^[43]

$$V_R = \frac{\varepsilon r_i r_j (\zeta_i^2 + \zeta_j^2)}{4(r_i + r_j)} \left\{ \frac{2\zeta_i \zeta_j}{\zeta_i^2 + \zeta_j^2} \ln \left(\frac{1 + \exp(-\kappa L)}{1 - \exp(-\kappa L)} \right) + \ln [1 - \exp(-2\kappa L)] \right\} \quad (13)$$

where ε is the permittivity of the medium, $L = R - (r_i + r_j)$ is the distance between the surfaces of the two particles and κ is the Debye-Huckel parameter given by

$$\kappa = \sqrt{\frac{8\pi N_A I e^2}{\varepsilon k_B T}} \quad (14)$$

It is worth pointing out that this approximation (Eq. 14) is invalid for the conditions of thick double layers (e.g., small ionic strength).

When the concentration of surfactant is below the critical micellar concentration (CMC), the fractional coverage of surfactant on latex particles can be estimated from the adsorption isotherm and the mass balance of the surfactant as ^[11]

$$\theta = f(C_{s, \text{aq}}) \quad (15)$$

$$C_{s, \text{tot}} = C_{s, \text{aq}} + A_{\text{ps}} \theta C_{s, \text{psat}} \quad (16)$$

where $C_{s, \text{tot}}$ is the total surfactant concentration in the vessel, $C_{s, \text{aq}}$ is the surfactant concentration in the aqueous phase, A_{ps} is the total particle surface per unit volume of the medium and $C_{s, \text{psat}}$ is the saturated concentration of adsorbed surfactant on the particle surface. Under the conditions of low surfactant concentration (i.e., sub-micellar surfactant concentration), such as in a coagulator, as a first approximation it is reasonable to assume that all the surfactant is adsorbed onto the surface of the latex particles. Therefore, the fractional coverage of surfactant can be evaluated as ^[11]

$$\theta = \frac{C_{s, \text{tot}}}{A_{\text{ps}} C_{s, \text{psat}}} \quad (17)$$

Under such conditions, the surface charge density of particles (σ_0) can be calculated as

$$\sigma_0 = \Theta_s \theta C_{s, \text{psat}} e N_A \quad (18)$$

where e is the charge of an electron and Θ_s is the valence of the surfactant.

The adsorption of counterions can be approximated by a Langmuir adsorption isotherm, which relates the adsorbed counterions ($C_{c,p}$) with the bulk concentration of the counterions ($C_{c,b}$) as ^[44]

$$\frac{C_{c,p}}{\theta C_{s,psat}} = \frac{\sigma_i}{\sigma_0} = \frac{KC_{c,b} \exp\left(\frac{z_c e \phi_1}{k_B T}\right)}{1 + KC_{c,b} \exp\left(\frac{z_c e \phi_1}{k_B T}\right)} \quad (19)$$

where $C_{c,p}$ is the concentration of adsorbed counterions on the particle surface, K the constant for the Langmuir adsorption equilibrium, Θ_c the valence of the counterion and $\sigma_i = z_c C_{c,p} e N_A$.

2.3 Ionic strength evaluation

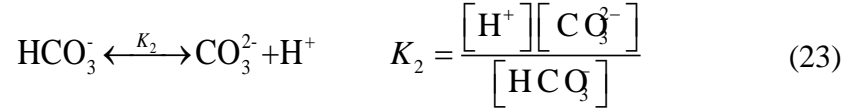
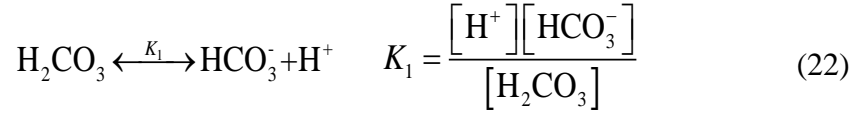
Several chemical species are involved in the present system, including the initiator (e.g. $\text{Na}_2\text{S}_2\text{O}_8$), a buffer (e.g. Na_2CO_3), a surfactant (SDS) and a coagulant salt (NaCl). The bulk concentration of all the ions is required in the calculation of the ionic strength. The species concentration is composed of three parts: the bulk concentration $C_{i,b}$, the adsorbed concentration $C_{i,p}$ and the concentration in the diffuse layer $C_{i,d}$. The only cationic species considered in this work is Na^+ because the concentration of H^+ is very small. Furthermore, the concentration of anionic species in the diffuse layer is small due to Donnan exclusion ^[11]. The distribution of Na^+ across the particle surface, the diffuse layer and the bulk aqueous solution is accounted for as

$$C_{\text{Na,tot}} = C_{\text{Na,b}} + C_{\text{Na,d}} + C_{\text{Na,p}} A_{ps} = C_{\text{Na,b}} + \theta C_{s,psat} A_{ps} \quad (20)$$

As the anions are not adsorbed, the balance for the anionic species (except for the surfactant) is

$$C_{i,\text{tot}} = C_{i^-,b} \quad (21)$$

In addition, the presence of Na_2CO_3 as the buffer affects the ionic strength as well. In this case, the association and dissociation of CO_3^{2-} are accounted for assuming equilibrium conditions.



The equation system of mass balance is completed by the existence of the electro-neutrality condition as

$$\sum_{i^+} \Theta_{i^+} C_{i^+,b} + \sum_{i^-} \Theta_{i^-} C_{i^-,b} = 0 \quad (24)$$

After solving the bulk concentration of each ionic species, the ionic strength can then be calculated as

$$I = 0.5 \times \sum_i \Theta_i^2 C_{i,b} \quad (25)$$

2.4 Rheology modeling

The emulsion latex with a solid content above $\sim 28\%$ exhibits typical shear-thinning behavior^[3]. A previous study from our laboratory^[45] showed that the Carreau-Yasuda model correctly captures the shear thinning behavior of latexes and so it was used in this work

$$\eta(\dot{\gamma}) = \eta_{\infty} + \frac{\eta_0 - \eta_{\infty}}{\left[1 + (\dot{\gamma}\tau)^a\right]^{(1-m)/a}} \quad (26)$$

where η_0 is the zero-shear viscosity, η_{∞} is the infinite-shear viscosity, τ is the characteristic time for the onset of shear-thinning, a and m are parameters. It was suggested that $a=1.0$ and $m=0.65$ provided the best fit to the corresponding experimental data ^[45]. The values of η_0 and η_{∞} can be estimated from Eqs. (27) & (28) ^[46]

$$\eta_0 = \eta_s \left(1 - \frac{\phi}{\phi_{m,\eta_0}}\right)^{-[\eta_0]\phi_{m,\eta_0}} \quad (27)$$

$$\eta_{\infty} = \eta_s \left(1 - \frac{\phi}{\phi_{m,\eta_{\infty}}}\right)^{-[\eta_{\infty}]\phi_{m,\eta_{\infty}}} \quad (28)$$

where η_s is the viscosity of the continuous phase, ϕ the latex solid content, ϕ_{m,η_0} the effective maximum packing fraction in the absence of shear and $\phi_{m,\eta_{\infty}}$ the effective maximum packing fraction under extreme shear. The intrinsic viscosities $[\eta_0]=4.2$ and $[\eta_{\infty}]=2.5$ ^[47].

The value of τ can be estimated from Eq. (29) ^[46]

$$\tau = \tau_s \left(1 - \frac{\phi}{\phi_{m,\eta_0}}\right)^{-[\eta_{\tau}]\phi_{m,\eta_0}} \quad (29)$$

where τ_s is the relaxation time for the continuous medium (at zero solids content) and $[\eta_{\tau}]=7.0$ ^[47].

As the particles do not have the same size, the effective packing fractions required to calculate the viscosity are calculated as ^[4]

$$\phi_{m,x} = \frac{\sum_{i=1}^m D_i^3 f_i}{\sum_{i=1}^m (D_i : \bar{D})^3 f_i + \frac{1}{\bar{n}} \sum_{i=1}^m [(D_i + \bar{D})^3 - (D_i : \bar{D})^3] f_i} \quad x = \eta_0, \eta_\infty \quad (30)$$

where the average number of spheres sharing the common space (\bar{n}) is given by

$$\bar{n} = 1 + \frac{4}{13} \bar{D} \frac{\sum_{i=1}^m (8\phi_{m,i} - 1)(D_i + \bar{D})^2 \left(1 - \frac{3}{8} \frac{\bar{D}}{D_i + \bar{D}}\right) f_i}{\sum_{i=1}^m [D_i^3 - (D_i : \bar{D})^3] f_i} \quad (31)$$

$$\text{and } (D_i : \bar{D}) = \begin{cases} 0 & \text{for } D_i \leq \bar{D} \\ D_i - \bar{D} & \text{for } D_i > \bar{D} \end{cases} \text{ and } f_i = \frac{\phi_i / D_i^3}{\sum_{i=1}^m \phi_i / D_i^3}.$$

where D is the particle diameter and the number average diameter \bar{D} is calculated by

$$\bar{D} = \sum_{i=1}^m D_i f_i \quad (32)$$

There is a stabilization layer surrounding the individual latex particle, so the particle is actually not hard sphere but deformable sphere under shear^[48]. Therefore, the effective volume fraction of the latex particles can be greater than the volume fraction of the solid particles alone. The thickness of the stabilizing layer is estimated by the Debye length (κ^{-1}) such that the effective maximum packing fraction of a particle with radius r_i can be computed as

$$\phi_{m,i} = \phi_{m,hs} \left(1 + \frac{1}{\kappa r_i}\right)^3 \quad (33)$$

where $\phi_{m,hs}$ is the volume fraction of the solid particles alone, without the double layer,

$\phi_{m,hs} = 0.64$ in the absence of shear^[49] and $\phi_{m,hs} = 0.71$ at high shear limits^[45, 50].

3. Method

3.1 Coagulator Geometry and Latex System

It was found relevant to check if the coagulator bottom shape has an effect on the latex coagulation process, therefore, two typical coagulators were considered, namely a flat-bottomed cylindrical stirred vessel and one with a curved-bottom. Both tanks have a diameter of TT with four vertical baffles of width $BT=TT/10$ mounted equally-spaced to the vessel wall. A standard Rushton turbine with diameter of $DI=TT/3$ was used. Other dimensions $HT=TT$ and $CI=TT/3$ are labeled in Figure 2. The inlet and outlet are installed opposite to each other midway between two consecutive baffles at height $z_{inlet}=0.8HT$ and $z_{outlet}=0.15HT$, respectively. Three coagulators with different sizes were considered, namely, $TT_1=0.18$ m (Coagulator 1), $TT_2=0.36$ m (Coagulator 2) and $TT_3=1.44$ m (Coagulator 3), to examine how scale-up impacts the latex particle coagulation processes in coagulators.

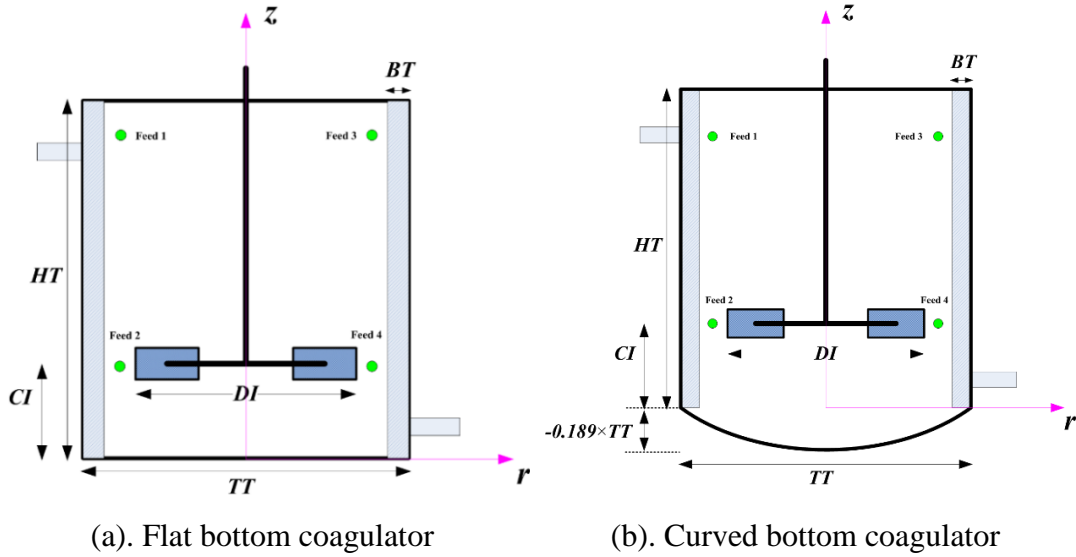


Figure 2. Schematic of the coagulator geometry

(Feed 1 & Feed 3: $r_f=TT/4$ and $z_f=0.86HT$;

Feed 2 & Feed 4: $r_f=TT/4$ and $z_f=0.33HT$).

The relevant latex parameters are given in Table 1. The salt solution of NaCl with known concentration was continuously fed into the coagulator at a well-controlled flow rate. The coagulation process was carried out at constant temperature at $T=308.15$ K.

Table 1. Model parameters and latex properties [40].

Hamaker constant (A, J)	5.5×10^{-21}	Solid weight fraction	0.303
Outer Stern layer thickness (δ , nm)	0.14	Initial average particle diameter (nm)	150 ~ 240
Langmuir adsorption constant ($K, \text{m}^3/\text{mol}$)	9.0×10^{-3}	Initial particle number concentration ($\#/ \text{m}^3$)	1.7×10^{20}
Critical micellar concentration (mol/m^3)	1.77	Surfactant (SLS) concentration (mol/m^3)	20
Saturated surfactant concentration at particle surface ($C_{s,psat}, \text{mol}/\text{m}^2$)	4.74×10^{-6}	Initiator (NaPS) concentration (mol/m^3)	20
Dissociation constant (K_1)	4.5×10^{-4}	Additive (Na_2CO_3) concentration (mol/m^3)	9.0
Dissociation constant (K_2)	4.7×10^{-8}	NaCl concentration (mol/m^3)	18.6

3.2 CFD model description

The geometry of coagulator was generated by using open source platform *Salome*. The computational mesh was generated with *SnappyHexMesh* on the open source platform OpenFOAM. An inner zone and an outer zone separated by an interface was created for the treatment of the impeller rotation. The multiple frames of reference (MFR) technique was adopted to deal with the impeller rotation, which directly modelled the inner zone in a rotating frame of reference and the outer zone in a stationary frame of reference. The MFR method represents a good compromise between reasonable

computational effort and physical accuracy. Since the latex particles are on the scale of nanometers, the particles follow the liquid motion closely. The Reynolds-Averaged Navier Stokes (RANS) approach coupled with the $k-\varepsilon$ model was used to model the flow, which has been shown to provide good agreement with experimental results^[51, 52]. The following boundary conditions were applied: (I) constant angular velocity along the impeller surface; (II) no slip condition at the baffles and along the vessel wall; (III) no normal velocity at the fluid surface, which was assumed to be flat. The simulations were considered to be converged when the normalized residuals drop below 10^{-4} .

3.3 Species mixing model

The species mixing process was calculated by using the resolved flow field. The transport equation for chemical species is given by

$$\frac{\partial(\rho C_i)}{\partial t} + \nabla \cdot \rho \mathbf{u} C_i = \nabla \cdot (\Gamma_{\text{eff}} \nabla C_i) \quad (34)$$

where $\Gamma_{\text{eff}} = D_{\text{mol}} + \Gamma_t$. The turbulent diffusivity is computed by dividing the turbulent kinetic viscosity (ν_t) by the turbulent Schmidt number as $\Gamma_t = \nu_t / Sc_t$ and $Sc_t = 0.7$ and $D_{\text{mol}} = 2.29 \times 10^{-9} \text{ m}^2/\text{s}$ were used in this work^[53, 54]. The time step for the transient species mixing simulation was $1 \times 10^{-4} \text{ s}$. The boundary condition for the species mixing calculation was zero flux at the solid walls. The initial condition was the species concentration equals to the feeding concentration at the feeding location while zero elsewhere in the coagulator. The PBE (Eq. (1)) was solved by means of the fixed pivot algorithm [55] based on the obtained flow field and the corresponding species mixing result in this work.

4. Results and Discussion

4.1 Flow model validation

The flow model was assessed by simulating the experiment by Wu and Patterson^[56], in which they measured by means of laser Doppler anemometry (LDA) technique the flow velocity distribution driven by a Rushton turbine with a flat bottom in a single phase cylindrical flat-bottom stirred tank ($TT=0.27$ m, $BT=TT/12$, $DI=0.093$ m, $CI=T/3$, $N=200$ rpm). Their experimental conditions were replicated as closely as possible in order to validate the flow model in this work. The comparisons of the predicted mean velocity components with the LDA measurements^[56] are illustrated in Figure 3. As seen, the results predicted from the present flow model were in good agreement with the measured data, which validates our flow model.

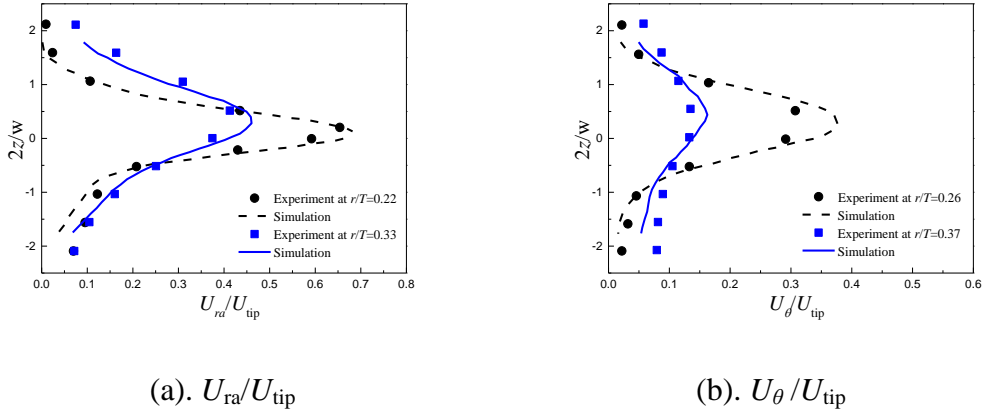


Figure 3. Comparison between simulated mean velocity components in a stirred tank with corresponding experimental data from the literature. (a) Dimensionless radial velocity component (U_{ra}/U_{tip}), (b) Dimensionless tangential velocity component (U_{θ}/U_{tip}).

4.2 Mixing process

The feeding of NaCl solution plays a controlling role in triggering the particle coagulation in the coagulators, as the latex coming out of the emulsion polymerization reactor is generally stable. A visual representation of the evolution of NaCl concentration is shown in Figure 4. The inlet and outlet flow rate for the considered coagulator was 4.58 L/min. The NaCl was injected instantaneously into the coagulator with a concentration of 18.6 mol/m³.

(c). $t=3.4$ s

(d). $t=5.6$ (s)

Figure 4. Variation of NaCl concentration in a coagulator with time .

The coagulator operates in a continuous mode, the profile of NaCl concentration would reach a steady state, which was then used as input into the coagulation model.

4.3 Coagulation mechanisms

Strictly speaking, the particle coagulation is a result of the combined effect of perikinetic and orthokinetic mechanisms in a practical coagulator. It is of interest to examine the relative magnitude of each mechanism for practically useful operating conditions in the coagulators^[40]. Usually this was determined via the evaluation of the particle Peclet number (Pe) (Eq. (5)). In the case of $Pe \ll 1$, the perikinetic mechanism dominates the coagulation process; while in the case of $Pe \gg 1$, it can be assumed that orthokinetic mechanism governs the coagulation process; when $Pe \sim 1$, both mechanisms are equally important^[57]. However, Melis et al.^[40] suggested that the ionic strength should be accounted for the evaluation of relative importance of orthokinetic coagulation to perikinetic coagulation, and they proposed the modified Peclet number as calculated by Eq. (6). For this, they suggested $Pe' < 0.1$ as an

approximate criterion for the coagulation rate to be governed by the perikinetic mechanism, and $Pe' > 0.1$ as a criterion for the coagulation rate to be dependent on the orthokinetic mechanism. Therefore, the values of Peclet number (Pe) and modified Peclet number (Pe') versus particle pair for the latex system used in this work are plotted in Figure 5.

(a). *Pe versus particle diameter.*

(b). *Pe' versus particle diameter*

Figure 5. Peclet number and modified Peclet number versus particle size for the System ($N=500$ rpm).

As seen from Figure 5, the value of Pe is small ($\ll 1$) when the particles are smaller than about 400 nm, the value of Pe becomes bigger (~ 1) when the sizes of particles increase (> 400 nm). The value of the modified Peclet number Pe' is very small ($\sim 10^{-3} \ll 0.1$) over the entire range of particle sizes. This is because of the relatively high value of ionic strength in this example, which leads to κr values ranging between 75 and 100. The coagulation process was governed by the perikinetic mechanism in the coagulator under the considered agitation rate and electrolyte concentration. Induced coagulation thus requires a modification of the ionic strength, while the shear effect seems to be negligible under the considered conditions.

To further investigate if the shear effect could be ignored in such systems, the stability ratio calculated from Eq. (3) as a result of Brownian motion is shown in Figure 6(a) and the stability ratio calculated from Eq. (4) as a result of the combined effect of Brownian motion and fluid motion is shown in Figure 6(b). It can be seen that both

equations gave similar values. It can be noticed also that the stability ratio between a pair of bigger particles is larger than that between a pair of smaller particles.

(a). $\log_{10}(W_{ij})$ versus d_p

(b). $\log_{10}(W_{ij,com})$ versus d_p

Figure 6. The dependence of $\log_{10}(W_{ij})$ and $\log_{10}(W_{ij,Com})$ on the particle sizes ($N=500$ rpm).

4.4 Coagulation model validation

The experimental data from Melis et al. ^[11] was used to validate the adopted coagulation model as it provided a complete list of physico-chemical parameters that was needed in the implementation of the coagulation model. The simulation was carried out in a way of replicating their experiment as closely as possible. In their experiment, the particles started to coagulate after increasing the sodium chloride concentration to 16 mol/m³. They frequently recorded the evolution of the mean particle diameter and total particle number with time as shown by the scattered points in Figure 7. The simulation results are shown alongside with their experimental data in Figure 7. The experimental results showed that very rapid particle coagulation occurs in the first few minutes, and then the coagulation process became slow. This was because the addition of salt solution of NaCl instantaneously decreased the zeta potential from about 32.4 to 28.2 mV, which destabilized the latex by coagulating the particles to reduce the total particle surface. As the total particle surface decreased, the surface charge density increased and the zeta potential reached 30 mV. Gradually, a new stable latex system could be reached again. It is seen from the comparisons that the

present coagulation model has captured the trends of variation satisfactorily, which provides good confidence in the implemented perikinetic coagulation model.

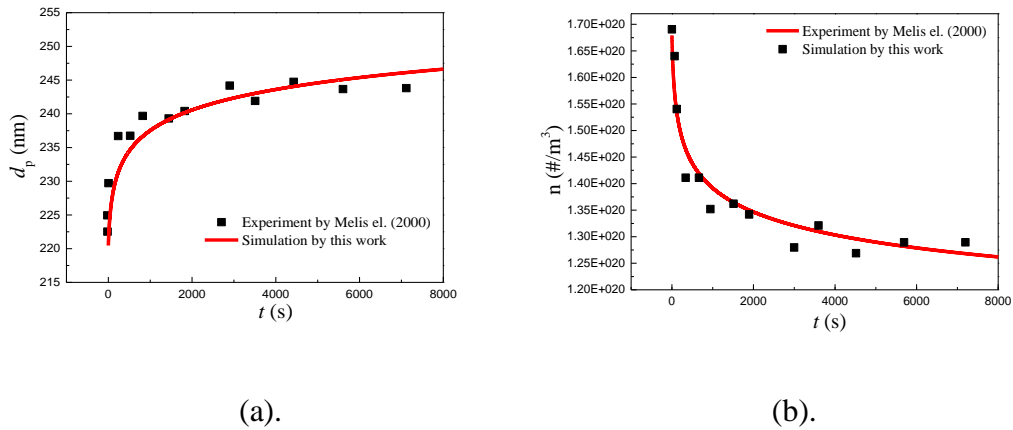


Figure 7. Evolution of particle diameter and number with time after adding 16 mol/m³ NaCl solution. (a) Variation of average particle diameter, (b) Variation of total particle number

4.5 Effect of the Tank Bottom

The influence of two typical tank bottoms on particle coagulation was examined. The contour of the particle size at a vertical plane middle way between two consecutive baffles is shown in Figure 8. It is important to remind that the NaCl was injected continuously from the location of Feed 1.

(a). Flat bottom coagulator (b). Curved bottom coagulator

Figure 8. Contour plot of particle size resulted from two typical tank bottoms of Coagulator 1 with $TT_1=0.18$ m at $N=380$ rpm.

Figure 8 shows that the size distributions are very similar for both two tanks. The mean particle size at the outlet was 216 nm for the flat-bottom coagulator and 212 nm

for the curved-bottom one (the mean size of the latex entering the coagulator was 160 nm), which suggested that the shape of the bottom plays only a small role in affecting the latex coagulation process. Since the results from the two typical tanks were close to each other and the flat bottomed stirred tank was extensively used as a standard configuration in the literature, so the flat-bottom tank was used hereafter in this work.

4.6 Effect of the Salt Solution Feed Position

The effect of salt solution feed position was evaluated by considering four feeding locations, namely Feed 1, Feed 2, Feed 3 and Feed 4 labeled in Figure 2. The contour of particle size at a vertical plane middle way between two consecutive baffles is shown in Figure 9.

Figure 9. Contour plot of particle size resulted from feeding at different locations of Coagulator 2 with $TT_3=1.44$ m at $N=425$ rpm.

It is seen that the size distribution was almost the same for the four contour plots, but there was a difference in the maximum value of the particle diameter. The maximum value of particle diameter was more or less the same when injecting from Feed 1, Feed 2 and Feed 3, while it was larger than that that feeding from Feed 4. The average particle size at the coagulator outlet is quantitatively compared in Figure 10. The smallest particles were produced by feeding from Feed 4. This can be explained by the fact that the location of Feed 4 was positioned close to the coagulator outlet and therefore part of the NaCl solution was evacuated directly before mixing into the

coagulator, which led to a lower NaCl concentration in the coagulator and thus to a lower extent of particle coagulation.

Figure 10. Effect of Feed Location for Coagulator 2 at $N=425$ rpm.

The results illustrated that the overall influence of salt solution feeding location may not be the main concern of such unit operating under these particular conditions, while feeding the salt solution near the reactor outlet should be avoided. As it is practically more convenient to feed from top, so the Feed 1 was used hereafter in this work.

4.7 Effect of the scale-up criterion

Three sizes of coagulators were considered with $TT_1=0.18$ m (Coagulator 1), $TT_2=0.36$ m (Coagulator 2) and $TT_3=1.44$ m (Coagulator 3) to examine how scale-up impacts the latex particle coagulation processes in coagulators. The scale-up ratio was up to 512:1 ($V_{\text{Coagulator 3}}/V_{\text{Coagulator 1}}$), which was considered large enough to quantitatively explore the scale-up effect in such applications.

The Coagulator 1 represented the typical lab-scale coagulator, while the Coagulator 3 represented the typical pilot-scale coagulator. Four scale-up strategies were examined in this work ($N_1=378$ rpm for Coagulator 1):

(1). Equal mixing time and geometrical similarity:

$$\theta_{\text{mix}} \propto \frac{1}{N_1} \quad (35)$$

$$N_2 = N_1 \quad (36)$$

(2). Equal power input per unit volume and geometrical similarity:

$$\frac{P}{V} \propto N^3 DI^2 \quad (37)$$

$$N_2 = N_1 \left(\frac{DI_1}{DI_2} \right)^{\frac{2}{3}} \quad (38)$$

(3). Equal impeller tip velocity and geometrical similarity:

$$N_2 = N_1 \left(\frac{DI_1}{DI_2} \right) \quad (39)$$

(4). Equal impeller Reynolds number and geometrical similarity:

$$N_2 = N_1 \left(\frac{DI_1}{DI_2} \right)^2 \quad (40)$$

Different criteria are mutually exclusive, as it is impossible to maintain all the parameters in the same ratio to one another. The different scale-up criteria often resulted in different process conditions on a larger scale. The mean particle sizes at the coagulator outlet from the four criteria are compared in Figure 11.

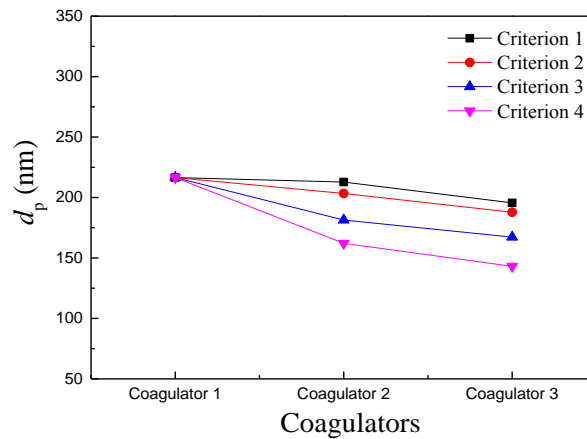


Figure 11. Effect of scale up criteria on the mean particle size at the coagulator outlet.

It is seen that the size of particles decreased when scaled up by any of the four criteria. In other words, small scale coagulators appeared to be more efficient than larger ones. While Criterion 1 and Criterion 2 show very similar results, Criterion 1 gave the largest particles (with less difference at smaller scales), and the Criterion 4 produced the smallest particles in larger coagulators (with big difference compared to smaller scales).

The effect of the four scale-up criteria on the particle size distributions from the outlet of Coagulator 3 is shown in Figure 12. It is of interest to see that the distributions from Criterion 3 and Criterion 4 are wider than those from Criterion 1 and Criterion 2, and they exhibit approximately a bimodal pattern.

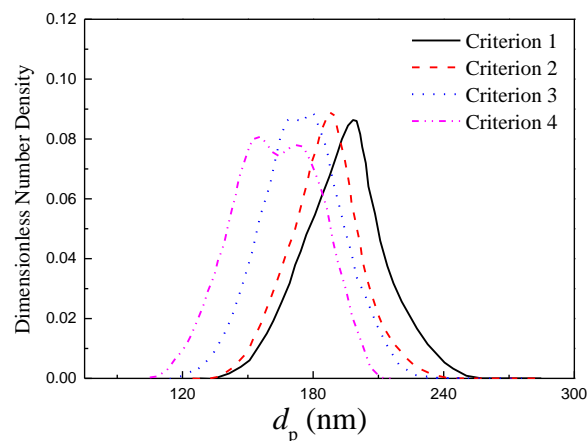


Figure 12. Effect of scale-up criteria on the particle size distributions from the outlet of Coagulator 3.

The mixing condition played a significant role in the process of emulsion latex coagulation, as shown by the steady-state mixing conditions in Figure 13.

Figure 13. Steady-state mixing contour of NaCl concentration by the four scale-up criteria for Coagulator 2.

The scale-up based on Criterion 1 (i.e., constant impeller speed) increased the P/V , maximum shear rate and Reynolds number, which effectuated a better mixing throughout the reactor (see Figure 13(a)). This criterion thus produced the largest particles (see Figure 11). However, this criterion is not realizable in practice as high mixing speeds in big reactors cause hazardous vibrations and consume much more energy than really needed. In the present work, the P/V for Coagulator 3 was 16 times as large as that for coagulator 1 via constant impeller speed scale-up.

The scale-up based on Criterion 2 (i.e., constant P/V) maintained similar mixing throughout the coagulator (see Figure 13(b)), but increased the maximum shear rate and Reynolds number. Therefore, this criterion seemed to be a good criterion for scaling up of emulsion latex coagulators.

Scaling up Coagulator 1 by means of Criterion 3 and Criterion 4 resulted in a very low value of P/V in Coagulator 3, which was only a small fraction of the P/V value in Coagulator 1. Therefore, the Criterion 3 and 4 can hardly be a good scale-up criterion, because a very low P/V value provokes a deficient mixing as shown in Figures 13 (c) and (d).

Scale up from lab scale to industrial scale installation consists of a series of complex tasks. Useful information can be learned from CFD simulations, though, it hardly can fully replace the step-by-step pilot procedures. Often, the trial and error method still needs to be included in practice, but the amount of experimental tests can be reduced.

4.8 Effect of the residence time

Simulations were carried out to study the impact of the mean residence time on the coagulated average particle size. In order to do so, the latex flow rate was modified

while keeping the same ratio of NaCl flow rate to the latex flow rate. The average particle diameter at the outlet versus the mean residence time is plotted in Figure 14.

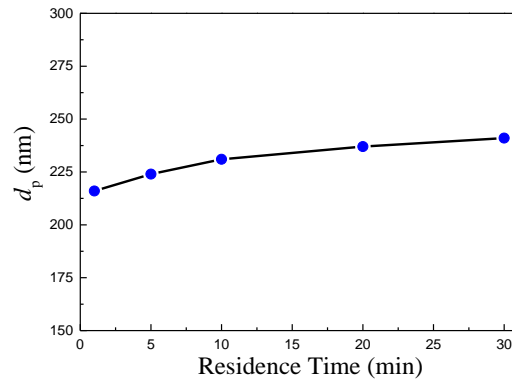


Figure 14. Effect of the mean residence time on the particle size in Coagulator 1 at $N=378$ rpm.

A small latex flow rate leads to a high residence time, while a large flow rate leads to a low residence time. At very low residence time, the latex and the salt fed into the reactor were poorly mixed, and the mixing behavior deviated largely from the ideal CSTR assumption. In contrast, the homogeneity of salt species throughout the coagulator becomes pronounced at high residence time. Besides, at high residence time, the particles can stay inside the coagulator longer, and grow for a longer time inside the reactor, so the particle size increased.

4.9 Effect of the agitation speed

The effect of the agitation intensity on the coagulation process is plotted in Figure 15.

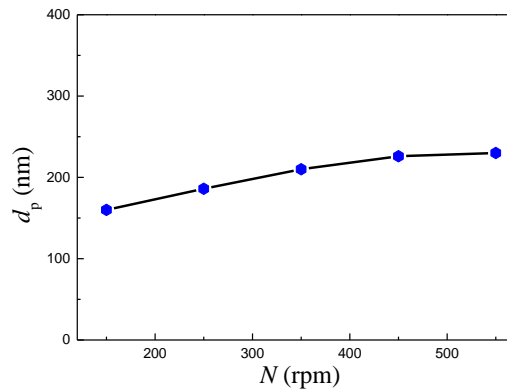


Figure 15. Effect of the agitation on the particle size in Coagulator 1.

The results show that the particle size increases with an increase in the impeller speed. A higher agitation intensity means faster and better mixing of salt species throughout the coagulator, which promotes coagulation process. If the mixing was already high enough to ensure fast homogeneity of the species, further increase in agitation (e.g. between 450 and 550 rpm) would only have a negligible effect on the coagulation process.

5. Conclusion

In this work, the emulsion latex coagulation processes in coagulators were numerically studied based on the full CFD approach. The RANS approach together with the $k-\varepsilon$ turbulence model was adopted to describe the detailed flow field in the coagulators. The coagulant mixing process was simulated by solving the convection-diffusion model and the latex coagulation process was described by the population balance equation together with a coagulation model. The flow model was independently validated by means of comparing simulated flow field to the corresponding experimental data from the literature. The latex coagulation model was benchmarked

against measured data from the literature in terms of evolution of average particle size and total number of particles.

A series of simulations were carried out to study the effects of relevant operating parameters and four typical scale-up criteria on the particle coagulation process in continuous latex coagulators. The results revealed that the shape of the coagulator bottom plays only a small role in affecting the latex coagulation process. As far as the feed location of coagulant was concerned, feeding the coagulant near the reactor outlet should be avoided. In addition, it was found that the size of particles decreases when the coagulator was scaled up by all the four criteria, the Criterion 1 gave the largest particles and the Criterion 4 produced the smallest particles in larger coagulators. Moreover, the particle size increased with the increase of the mean residence time (which can be explained by a longer exposure to collisions thus causing particle growth) as well as with the impeller speed. The results presented would be helpful for the relevant process design, development and scale-up.

Nomenclature

a	parameter
A	Hamaker constant
A_{ps}	total particle surface per unit volume of water, m^2/m^3
BT	baffle width, m
C	concentration, mol/m^3
CI	impeller clearance, m
CMC	critical micellar concentration, mol/m^3
d_p	particle diameter, nm
D_i	particle diameter, m
\bar{D}	particle number average diameter, m
DI	impeller diameter, m
e	charge of an electron
F	external force, N
G	shear rate, 1/s
H	hydrodynamic interaction function between two particles
HT	liquid height, m
I	ionic strength
IHP	inner Helmholtz plane
k_B	Boltzmann constant, J/K
K	the constant for the Langmuir adsorption equilibrium
K_1	Dissociation constant
K_2	Dissociation constant
K_s	capacitance of the layer
L	distance between the surfaces of the two particles, m
$n(V, t)$	number density function, $\#/m^3/m^3$
\bar{n}	average sphere packing coordination number
N	impeller agitation speed, rpm
N_A	Avogadro's number, $\#/mol$
NaPS	sodium persulfate
m	parameter

OHP	outer Helmholtz plane
P	power consumption, W
Pe	particle Peclet number
Pe'	modified particle Peclet number
r	radius of spherical particle, m; radial coordinate, m
R	center-to-center separation, m
Sc_t	turbulent Schmidt number
SLS	sodium laureth sulfate
t	time, s
T	temperature, K
TT	internal diameter of the coagulator, m
u	particle velocity, m/s
\mathbf{u}	flow field, m/s
U	velocity component, m/s
V	volume of particle, m ³
V'	volume of particle, m ³
V_0	smallest volume of particles, m ³
V_A	Van der Waals attractive potential energy, J
V_{int}	total inter-particle interactions, J
V_R	repulsive potential energy, J
W_{ij}	stability ratio
z	axial coordinate, m

Greek letters

α	collision efficiency
β	coagulation rate coefficient
δ	thickness of outer Stern layer, m
ε	turbulent kinetic energy dissipation rate, m ² /s ³ ;

	permittivity of the medium, F/m
ε_s	permittivity of the Stern layer, F/m
ϕ_0	electric surface potential at particle surface, V
ϕ_i	electric surface potential at the inner Helmholtz plane, V
$\phi_{m,hs}$	volume fraction of the solid particles alone, without the double layer
μ	dynamic viscosity, Pa·s
ν	kinetic viscosity, m ² /s
ν_t	turbulent kinetic viscosity, m ² /s
η_0	zero-shear viscosity, m ² /s
η_∞	infinite-shear viscosity, m ² /s
η_s	viscosity of the continuous phase, m ² /s
$\dot{\gamma}$	shear rate, 1/s
$\dot{\gamma}_m$	characteristic shear thickening time, s
κ	Debye-Huckel parameter, 1/m
k_B	Boltzmann constant, J/K
τ	the characteristic time for the onset of shear-thinning, s
τ_c	critical time for shear thickening of the continuous medium, s
τ_s	relaxation time for the continuous medium, s
ϕ	solid volume fraction
ϕ_{m,η_0}	effective maximum packing fraction in the absence of shear
ϕ_{m,η_∞}	effective maximum packing fraction under extreme shear
θ	fractional coverage of surfactant on the particle
$[\eta_0]$	intrinsic viscosity under zero shear, m ² /s
$[\eta_\infty]$	intrinsic viscosity under zero shear, m ² /s
σ_0	surface charge density, C/m ²
σ_i	charge density of the inner Helmholtz plane, C/m ²
σ_d	net charge density of outer Helmholtz plane, C/m ²
ζ	electrokinetic (zeta) potential, V

Θ	valence
χ	emulsifier coverage, mol/m ²
Γ_{eff}	effective diffusivity, m ² /s
ρ	density, kg/m ³

Subscripts

1, 2, 3	numbers
A	attraction
aq	aqueous solution
b	bulk concentration
c	counterion
Com	combined coagulation mechanism
d	diffuse layer
f	feed location
<i>i</i>	chemical species
<i>i, j</i>	<i>i</i> th , <i>j</i> th particle
<i>i</i> ⁺	cation
<i>i</i> ⁻	anion
inlet	coagulator inlet
int	total inter-particle interaction
max	maximal
mol	molecular
Na	sodium species
outlet	coagulator outlet
ra	radial direction

R	repulsion
s	surfactant
tot	total
p	adsorbed
ps	particle surface
psat	saturated concentration of adsorbed surfactant on the particle surface
θ	tangential direction

References

- [1] D. C. Blackley, *Polymer latices: Science and Technology. Vol. 1, Fundamental Principles*, Chapman & Hall, London, UK **1997**.
- [2] C. B. Chung, S. H. Park, I. S. Han, Y. H. Seo, B. T. Yang, *AIChE Journal* **1998**, *44*, 1256.
- [3] R. C. Elgebrandt, J. A. Romagnoli, D. F. Fletcher, V. G. Gomes, R. G. Gilbert, *Chemical Engineering Science* **2005**, *60*, 2005.
- [4] J. Pohn, M. Heniche, L. Fradette, M. Cunningham, T. McKenna, *Chemical Engineering & Technology* **2010**, *33*, 1917.
- [5] J. R. Richards, J. P. Congalidis, R. G. Gilbert, *Journal of Applied Polymer Science* **1989**, *37*, 2727.
- [6] C. Kiparissides, D. Achilias, E. Chatzi, *Journal of Applied Polymer Science* **1994**, *54*, 1423.
- [7] C. Kiparissides, I. Moustakis, A. Hamielec, *Journal of Applied Polymer Science* **1993**, *49*, 445.
- [8] E. Unzueta, J. Forcada, *Journal of Applied Polymer Science* **1997**, *66*, 445.
- [9] E. M. Coen, R. G. Gilbert, B. R. Morrison, H. Leube, S. Peach, *Polymer* **1998**, *39*, 7099.
- [10] E. M. Coen, S. Peach, B. R. Morrison, R. G. Gilbert, *Polymer* **2004**, *45*, 3595.
- [11] S. Melis, M. Kemmere, J. Meuldijk, G. Storti, M. Morbidelli, *Chemical Engineering Science* **2000**, *55*, 3101.
- [12] N. Lazaridis, A. Alexopoulos, E. Chatzi, C. Kiparissides, *Chemical Engineering Science* **1999**, *54*, 3251.
- [13] P. H. H. Araujo, J. C. de la Cal, J. M. Asua, J. C. Pinto, *Macromolecular Theory and Simulations* **2001**, *10*, 769.
- [14] J. Zeaiter, J. Romagnoli, G. Barton, V. Gomes, B. Hawket, R. Gilbert, *Chemical Engineering Science* **2002**, *57*, 2955.
- [15] C. D. Immanuel, C. F. Cordeiro, S. S. Sundaram, E. S. Meadows, T. J. Crowley, F. J. Doyle, *Computers & Chemical Engineering* **2002**, *26*, 1133.
- [16] C. D. Immanuel, F. J. Doyle, C. F. Cordeiro, S. S. Sundaram, *AIChE Journal* **2003**, *49*, 1392.
- [17] C. D. Immanuel, F. J. Doyle III, *Chemical Engineering Science* **2003**, *58*, 3681.
- [18] O. Kammona, P. Pladis, C. E. Frantzikinakis, C. Kiparissides, *Macromolecular Chemistry and Physics* **2003**, *204*, 983.
- [19] M. Fortuny, C. Graillat, T. F. McKenna, P. H. Araújo, J. C. Pinto, *AIChE Journal* **2005**, *51*, 2521.
- [20] M. Fortuny, C. Graillat, T. F. McKenna, *Industrial & Engineering Chemistry Research* **2004**, *43*, 7210.
- [21] M. T. Dokucu, M.-J. Park, F. J. Doyle, *Chemical Engineering Science* **2008**, *63*, 1230.
- [22] H. M. Vale, T. F. McKenna, *Industrial & Engineering Chemistry Research* **2009**, *48*, 5193.
- [23] F. J. Doyle, C. A. Harrison, T. J. Crowley, *Computers & Chemical Engineering* **2003**, *27*, 1153.
- [24] L. Krutzer, A. Van Diemen, H. Stein, *Journal of Colloid and Interface Science* **1995**, *171*, 429.

- [25] V. Lowry, M. El-Aasser, J. Vanderhoff, A. Klein, C. Silebi, *Journal of Colloid and Interface Science* **1986**, *112*, 521.
- [26] V. Lowry, M. S. El- Aasser, J. W. Vanderhoff, A. Klein, *Journal of Applied Polymer Science* **1984**, *29*, 3925.
- [27] A. Matějček, A. Pivoňková, J. Kaška, P. Dítl, L. Formánek, *Journal of Applied Polymer Science* **1988**, *35*, 583.
- [28] S. Ariaifar, *PhD Thesis, Univeristy Claude Bernard Lyon 1*, Lyon, France **2016**.
- [29] H. U. Moritz, *Chemical Engineering & Technology* **1989**, *12*, 71.
- [30] R. B. Bird, R. C. Armstrong, O. Hassager, *Dynamics of Polymeric Liquids. Vol. 1: Fluid Mechanics*, Wiley, New York, USA **1987**.
- [31] R. G. Larson, *The Structure and Rheology of Complex Fluids*, Oxford University Press New York, USA **1999**.
- [32] J. Pohn, M. Cunningham, T. F. McKenna, *Macromolecular Reaction Engineering* **2013**, *7*, 380.
- [33] J. Pohn, M. Cunningham, T. F. McKenna, *Macromolecular Reaction Engineering* **2013**, *7*, 393.
- [34] V. Smoluchowski, *Colloid & Polymer Science* **1917**, *21*, 98.
- [35] v. N. Fuchs, *Zeitschrift für Physik A Hadrons and Nuclei* **1934**, *89*, 736.
- [36] A. Zaccone, H. Wu, M. Lattuada, M. Morbidelli, *The Journal of Physical Chemistry B* **2008**, *112*, 6793.
- [37] A. Zaccone, H. Wu, D. Gentili, M. Morbidelli, *Physical Review E* **2009**, *80*, 051404.
- [38] D. Feke, W. Schowalter, *Journal of Fluid Mechanics* **1983**, *133*, 17.
- [39] D. Feke, W. Schowalter, *Journal of Colloid and Interface Science* **1985**, *106*, 203.
- [40] S. Melis, M. Verduyn, G. Storti, M. Morbidelli, J. Bałdyga, *AIChE Journal* **1999**, *45*, 1383.
- [41] E. J. W. Verwey, J. T. G. Overbeek, J. T. G. Overbeek, *Theory of the Stability of Lyophobic Colloids*, Elsevier, Amsterdam, the Netherlands **1948**.
- [42] R. Evans, D. H. Napper, *Journal of Colloid and Interface Science* **1973**, *45*, 138.
- [43] R. Hogg, T. W. Healy, D. Fuerstenau, *Transactions of the Faraday Society* **1966**, *62*, 1638.
- [44] J. Lyklema, *Fundamentals of Interface and Colloid Science*, Academic Press, London , UK **1995**.
- [45] M. Pishvaei, C. Graillat, T. McKenna, P. Cassagnau, *Journal of Rheology* **2007**, *51*, 51.
- [46] I. M. Krieger, T. J. Dougherty, *Transactions of the Society of Rheology* **1959**, *3*, 137.
- [47] M. Pishvaei, C. Graillat, T. F. McKenna, P. Cassagnau, *Polymer* **2005**, *46*, 1235.
- [48] A. Guyot, F. Chu, M. Schneider, C. Graillat, T. McKenna, *Progress in Polymer Science* **2002**, *27*, 1573.
- [49] R. Greenwood, P. F. Luckham, T. Gregory, *Journal of Colloid and Interface Science* **1997**, *191*, 11.
- [50] W. E. Smith, C. F. Zukoski, *Journal of Rheology* **2004**, *48*, 1375.
- [51] G. Montante, M. Moštek, M. Jahoda, F. Magelli, *Chemical Engineering Science* **2005**, *60*, 2427.
- [52] J. Aubin, D. F. Fletcher, C. Xuereb, *Experimental Thermal and Fluid Science* **2004**, *28*, 431.

- [53] H. Hartmann, J. Derksen, H. Van den Akker, *AIChE Journal* **2006**, *52*, 3696.
- [54] M. Coroneo, G. Montante, A. Paglianti, F. Magelli, *Computers & Chemical Engineering* **2011**, *35*, 1959.
- [55] S. Kumar, D. Ramkrishna, *Chemical Engineering Science* **1996**, *51*, 1311.
- [56] H. Wu, G. Patterson, *Chemical Engineering Science* **1989**, *44*, 2207.
- [57] D. Cheng, S. Ariaifar, N. Sheibat-Othman, J. Pohn, T. F. L. McKenna, *Polymer Reviews* **2018**, *58*, 717.

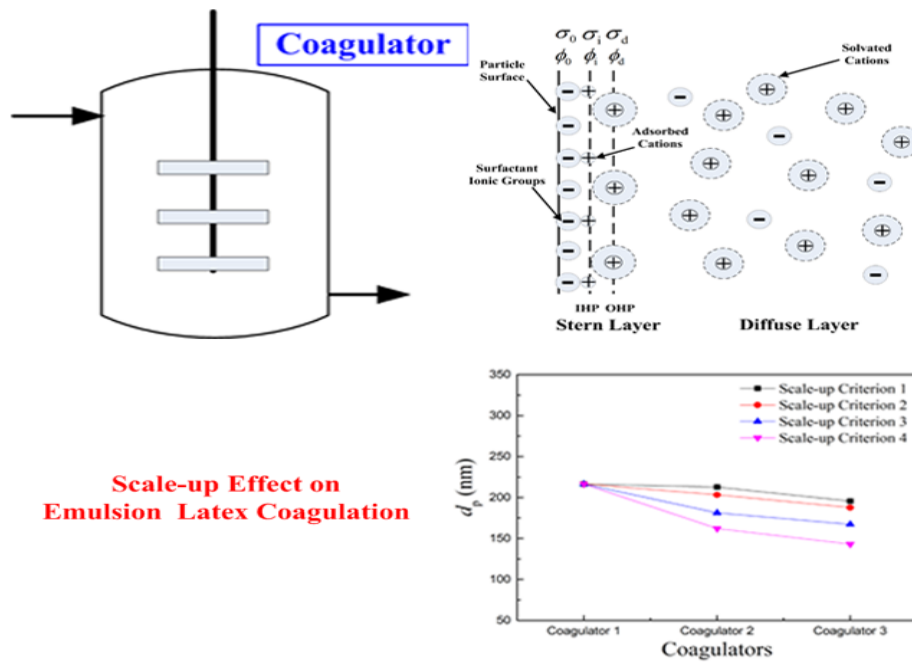


Table of Contents (TOC)

The CFD-based numerical simulation tool for emulsion latex coagulation process in coagulators was developed in this work. Numerical simulations were carried out to understand the influences of relevant operating parameters and the scale-up effect of four typical criteria on the continuous latex particle coagulation processes. The presented results would be helpful for the relevant process design, development and scale-up of continuous latex coagulators.